\$ SUPER

Contents lists available at ScienceDirect

Open Ceramics

journal homepage: www.sciencedirect.com/journal/open-ceramics





Production of fluorine-doped silica bodies using the optimized Vi-Si-HIP manufacturing process from the combination of viscous sintering and gas phase fluorination with subsequent hot isostatic pressing

L. Krämer *0, G. Falk

Institute of Structural and Functional Ceramics, Department of Materials Science and Engineering, Saarland University, D-66123 Saarbruecken, Germany

ARTICLE INFO

Keywords: Fluorination Silica Powder Temperature Hot isostatic pressing

ABSTRACT

A new manufacturing process aims to optimize the production of fluorine-doped glass in terms of energy efficiency. The green bodies are produced from nanoscale powders in a wet-chemical process and sintered at low temperatures in a fluorine-containing atmosphere. The green body composition and the sintering parameters such as gas atmosphere, temperature and feed rate are important for the resulting fluorine concentration and glass formation. The subsequent hot isostatic pressing leads to complete compaction of the sintered bodies and the associated increased transmission. By recompressing the samples, the sintering temperature can be lowered, thereby reducing the defluorination process at high sintering temperatures.

1. Introduction

In recent decades, the fluorination of glass has opened up a wide range of applications, for example in medical technology, spectroscopy and telecommunications. They are also frequently used in fiber lasers due to the high transmittable power [1–4]. When used in optical fibers, fluorination can ensure high numerical apertures. This makes it possible to use it as a minimally invasive surgical method in the medical technology, as the high numerical apertures enable a reduction in fiber diameter [4,5]. In addition, fluorine-doped glasses exhibit very good optical properties. The theoretical attenuation is 0.01 dB·km $^{-1}$ between 2 μm and 3 μm [1] In conventional vapor phase deposition systems, the fluorination is limited by the high process temperatures of over 2000 °C and the long process times [2,6].

The new Vi-Si-HIP process route is therefore required, which combines the viscous sintering (Vi-Si) of green bodies made of nanoscale SiO_2 powders in fluorine-containing gas atmospheres with subsequent post-compaction of the sintered bodies to form transparent, bubble-free glass bodies. The compaction is achieved by hot isostatic pressing of the sintered bodies in an inert gas atmosphere. Through the subsequent post-compaction, the sintering temperatures can be reduced to 1480 $^{\circ}$ C, which is a significant reduction compared to conventional production methods. The fluorination of the sintered body can be achieved by gasphase fluorination during sintering. The fluorine species and the fluorine

gas concentration are important factors.

The use of SF₆ gas in the sintering of SiO₂ bodies leads via

$$SF_6(g) + 3/2 SiO_2(s) \rightarrow 3/2 SiF_4(g) + SO_3(g)$$

to the formation of SiF4 gas, which can be used via

$$3 \text{ SiO}_2(s) + \text{SiF}_4(g) \leftrightarrows 4 \text{ O}_{3/2}\text{SiF}(s)$$

for the fluorination of the sintered body. The doping consists of a simultaneous process of fluorination and defluorination, which is also influenced by the process time and temperature [7–9].

The research focused on the production of fluorine-doped silica bodies using the innovative Vi-Si-HIP process route. Initially, green bodies with high densities and low porosities were produced via cast molding. The dispersions consisted of nanoscale SiO_2 powders and ammonium fluoride solution. The green bodies were then sintered in a tubular flow reactor under different gas atmospheres. The influence of gas phase fluorination was investigated. The sintered bodies were then hot isostatically pressed to achieve and confirm a reduction of bubbles in the glass.

2. Material and methods

Fig. 1 provides an overview of the process route. The molded bodies were obtained wet-chemically from nanoscale silica powder via casting

E-mail addresses: s9llkrae@stud.uni-saarland.de (L. Krämer), g.falk@nanotech.uni-saarland.de (G. Falk).

^{*} Corresponding author.

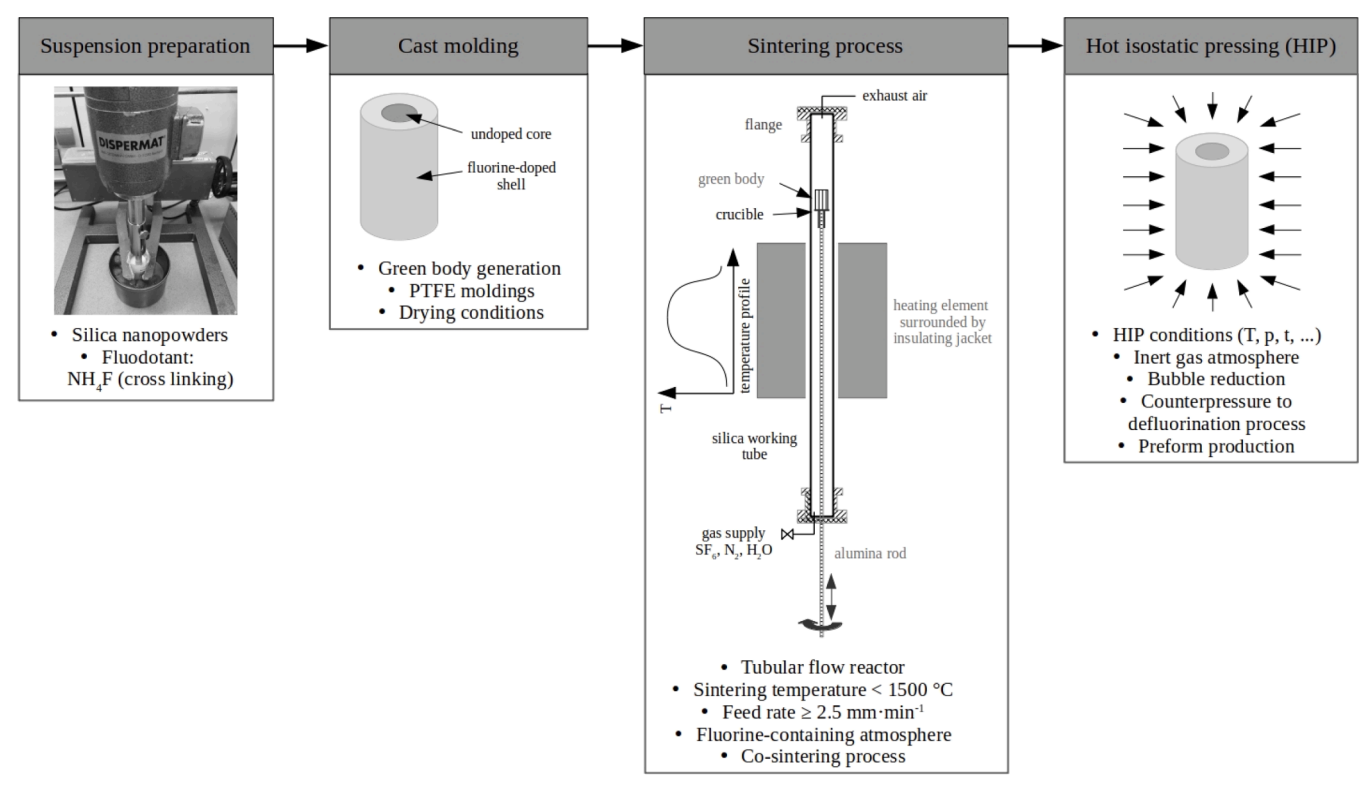


Fig. 1. Overview of the process route Vi-Si-HIP.

Table 1Details of the dispersion post-treatment.

Post-treatment	Details
Sieving	Screen mesh SEFAR $\ensuremath{\mathbb{R}}$ PET 1500 (Sefar AG), mesh size of 151 μm
Vacuum	Vacuum dissolver LDV-1 (PC Laborsystem GmbH) with a
dispersing	vacuum of -0.93 bar during dispersion for 10 min
Ultrasonic	ultrasonic sonotrode BRANSON Digital Sonifier ® W-450 D (G.
treatment	Heinemann Ultraschall- und Labortechnik, maximum power:
	400 W) with an amplitude of 30 % and a pulse and pause time of
	0.5 s each for 10 min

process. They were then compacted into a bubble-free SiO_2 glass body via zone sintering and subsequent hot isostatic pressing. The individual process steps are explained in more detail below.

2.1. Sample preparation

The green bodies were produced by dispersing the nanoscale $\rm SiO_2$ powder AEROSIL® OX50 (CAS: 112,945–52–5, Evonik Operations GmbH) in water with ammonium fluoride (NH₄F, CAS: 12,125–01–08, Sigma-Aldrich Chemie GmbH). The powder was stirred into the H₂O/NH₄F medium using the dissolver (Dispermat® N1, VMA-GETZMANN GmbH). The dispersion time was 10 min and was carried out under ice bath cooling. The dispersion has an NH₄F content of 0.38 ma. % and a filling grade of 50 ma. %.

In order to generate homogeneous green bodies with low porosity, further post-treatments of the dispersions were investigated in addition to dispersion. For this purpose, vacuum and ultrasonic treatment as well as sieving of the dispersion were carried out, see Table 1.

The casting was carried out in Teflon molds. After 24 h, the molds were demolded and dried in the digestorium under room conditions until the mass was constant.

2.2. Sample fluorination and sintering

The green bodies were sintered in a tubular flow reactor up to 1480 °C. The green body was moved through the furnace from top to bottom at a feed rate of 2.5 $\text{mm}\bullet\text{min}^{-1}$ to 10 $\text{mm}\bullet\text{min}^{-1}$. An additional gas atmosphere of SF₆ and N₂ was used to realize gas phase fluorination. Holding the sample in the hot zone for 3 h was also investigated. The fluorination and the sintering process were decisive.

2.3. Hot isostatic pressing

Post-compaction of pre-sintered OX50 samples was carried out using hot isostatic pressing (HIP). The OX50 sample was pre-sintered at 1480 $^{\circ}\text{C}$ with a feed rate of $10~\text{mm}\bullet\text{min}^{-1}$ in the tubular flow reactor. As a result, the pre-sintered sample still had some bubbles. The HIP process was designed to eliminate these bubbles. The process was carried out at Bodycote Specialist Technologies GmbH at a temperature of $1300~^{\circ}\text{C} \pm 10~\text{K}$ and a pressure of $100~\text{MPa} \pm 5~\text{MPa}$ under intert gas argon. The heating and cooling rate was $10~\text{K}\cdot\text{min}^{-1}$ and the holding time $180~\text{min} \pm 15~\text{min}$.

The inert gas exerts uniform, isostatic pressure on the glass. The temperature is set at a level that makes the glass viscous enough to eliminate bubbles, but does not cause deformation. After an optimized holding time, the pressure and temperature are slowly reduced. The result is defect-free, more homogeneous glass suitable for optical applications [10].

2.4. Sample characterization and analysis

The density, porosity and mean pore radius of the green bodies were determined using the Archimedes density method and the mercury porosity (porosimeter Pascal 440, Porotec, Germany).

Using the scanning electron microscope (SEM) Zeiss Sigma VP FEG-SEM at the Department of Materials Science and Methods (Saarland University), the sintered bodies could be examined topologically. Using

Table 2Density, porosity and mean pore radius of the green bodies, produced by dispersion with different post-treatment methods.

Dispersion post-	Archimedes	Mercury porosimetry		
treatment	$\rho \ / \ g{\cdot}cm^{-3}$	ρ/ g·cm ⁻³	Porosity / %	Average pore radius / nm
None	$1.141~\pm$	0.885 \pm	64.733 \pm	$31.379 \; \pm$
	0.007	0.012	1.051	0.631
Sieving	$0.870~\pm$	$0.803\ \pm$	59.335 \pm	32.473 \pm
	0.007	0.035	0.071	0.170
Vacuum	$0.886~\pm$	0.828 \pm	58.258 \pm	$32.256\ \pm$
dispersing	0.011	0.039	1.138	0.254
Vacuum	$0.881~\pm$	$0.838~\pm$	59.459 \pm	$31.863~\pm$
dispersing +	0.006	0.029	0.710	0.239
Sieving				
Ultrasonic	$0.930 \pm$	0.864 \pm	56.837 \pm	30.678 \pm
treatment	0.007	0016	0.897	0.268
Ultrasonic	$0.953 \pm$	0.897 \pm	57.309 \pm	29.227 \pm
treatment + sieving	0.010	0.007	1.103	0.487

the Oxford Instruments EBSD/EDS system, EDX spectra of the sintered bodies could also be recorded. Due to the low quantification accuracy of elements with atomic numbers below 10, the measurement of the fluorine concentration is evaluated critically [11], but can nevertheless give an indication of the sintering conditions.

The transmission of the OX50 samples before and after the HIP process was determined using UV/VIS spectroscopy (UV/Vis-NIR spectrometer Varian Cary 5E, Agilent Technologies).

3. Results and discussion

3.1. Dispersion preparation and green body characterization

The different preparation methods of the dispersions made it possible to achieve different densities, porosities and average pore radii in the green bodies, see Table 2. High densities and low porosities are crucial for improved sintering.

Without additional post-treatment of the samples, the green bodies had a density of $1.14~\rm g\cdot cm^{-3}$ (Archimedes), the porosity was approx. 65 % and the average pore radius was approx. 31 nm. The additional dispersion preparation with ultrasound and sieve made it possible to achieve reduced porosity (57 %) with relatively high density (0.95 $\rm g\cdot cm^{-3}$). The average pore radius was also reduced to approx. 29 nm. The vacuum treatment resulted in low densities and no reduction of the mean pore radii.

The deviation in density values between Archimedes' density determination and mercury porosimetry is due to the different measurement methods. Density determination using mercury porosimetry is less accurate, as it only determines the volume of pores accessible to mercury, i.e., connected and open pores, while closed pores and the actual total volume of the solid are not recorded. In addition, the assumption of ideally cylindrical pores is made. The Archimedes method, on the other hand, determines the apparent density, since the total volume, including all pores, is related to the mass due to the coating of the porous green body. The higher porosity and higher density measured using Archimedes' principle in the green bodies without additional processing methods can also be explained by the different measurement methods and the resulting measurement uncertainties.

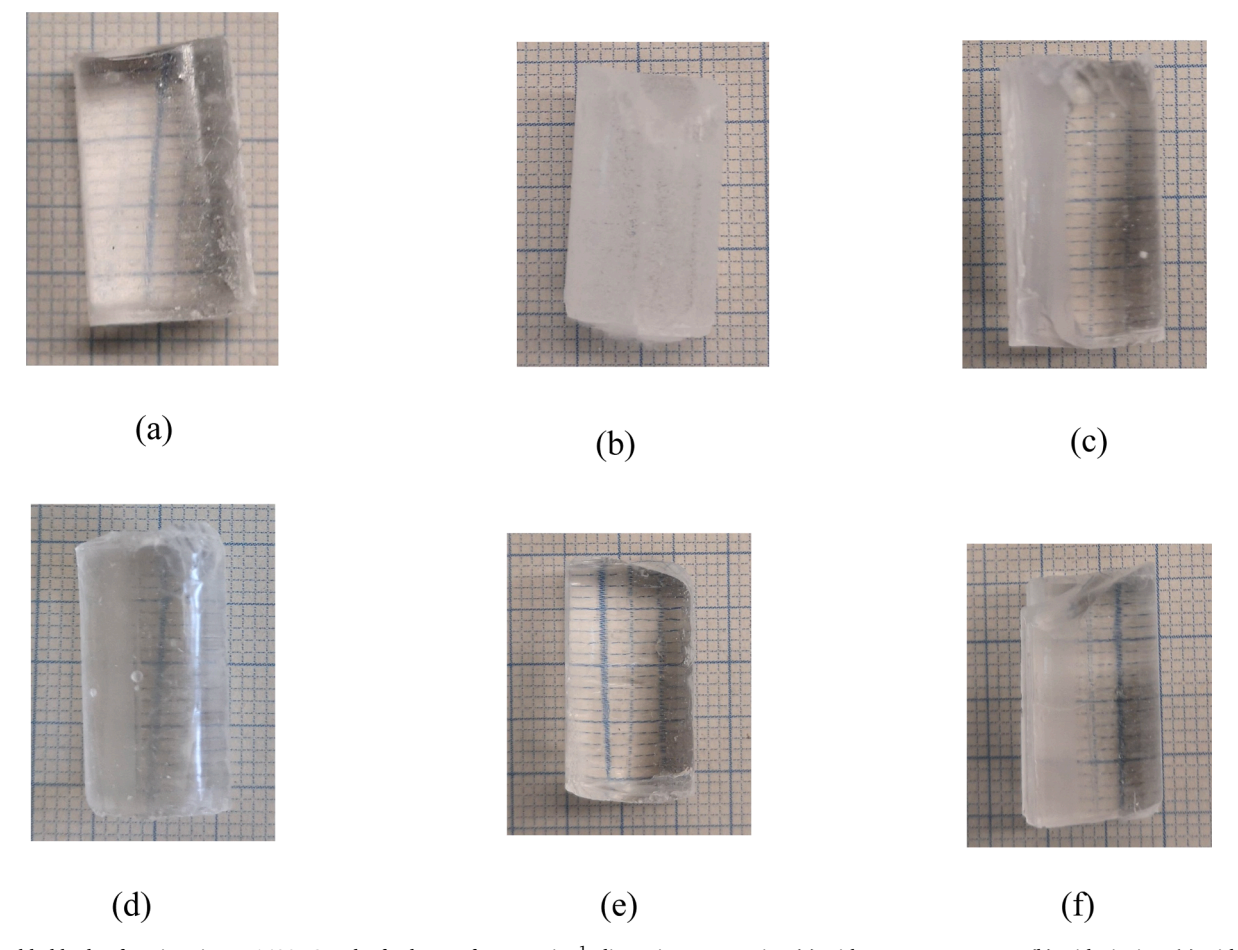
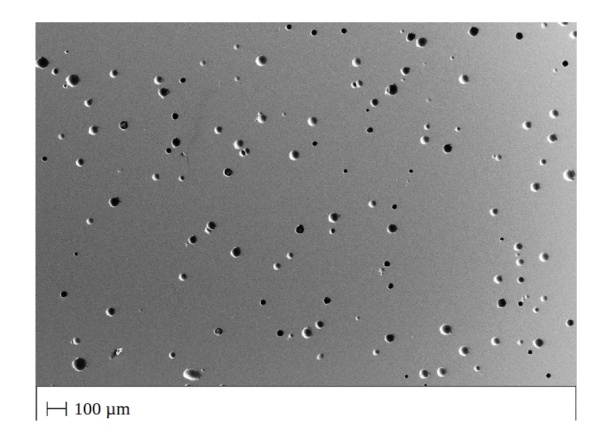


Fig. 2. Molded body after sintering at 1480 °C and a feed rate of 5 mm·min⁻¹: dispersion preparation (a) without post-treatment, (b) with sieving, (c) with vacuum dispersing, (d) with vacuum dispersing and sieving, (e) with ultrasonic treatment, (f) with ultrasonic treatment and sieving.

Table 3Cross-sections of the sintered bodies under different sintering conditions and sintering temperatures.

Sintering conditions	Gas atmosphere	1200 °C	1300 °C	1400 °C
3 h	$5~{ m ml_n\cdot min^{-1}~SF_6}, 50~{ m ml_n\cdot min^{-1}~N_2}$			
2.5 mm·min ⁻¹	$5~\text{ml}_\text{n}\text{·min}^{-1}~\text{SF}_6,50~\text{ml}_\text{n}\text{·min}^{-1}~\text{N}_2$			
	50 ml _n ·min ⁻¹ N ₂			



(a)

(b)

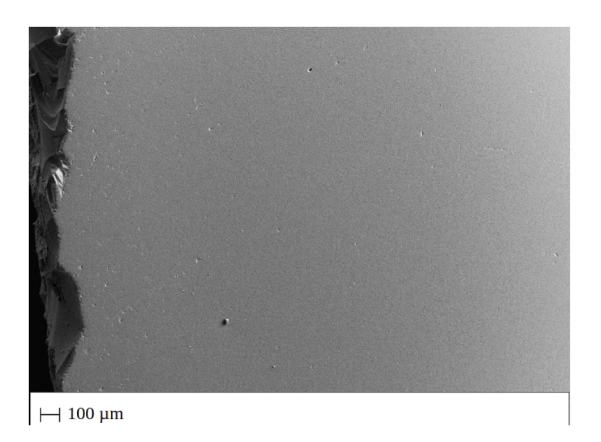


Fig. 3. SEM images of the molded bodies sintered under fluorine-containing furnace atmospheres at 1400 $^{\circ}$ C: (a) holding time 3 h, (b) feed rate 2.5 mm·min $^{-1}$.

The presence of large pores or cavities on the sample surface can also lead to measurement errors, especially in mercury porosimetry.

The reduced porosity and the small average pore radii should also improve the sintering result. The green bodies were therefore sintered at $1480\,^{\circ}\text{C}$ and a feed rate of $5~\text{mm}\cdot\text{min}^{-1}$ in the tubular flow reactor under a nitrogen atmosphere. The sintered moldings can be seen in Fig. 2.

The previous findings are supported by the sintering results. Low densities and high porosities lead to bubble-rich sintered bodies, see Fig. 2(b). Whereas a reduced porosity leads to transparent glass bodies. According to mercury porosimetry, the green body of sample 2 (a) has

Table 4EDX analysis of the sintered moldings under different sintering conditions and gas atmospheres in the flow reactor.

T /	Sintering	Gas atmosphere		Fluorine concentration
°C	condition	N_2 / $ml_n \cdot min^{-1}$	$SF_6 / ml_n \cdot min^{-1}$	/ ma %
1400	$2.5~\mathrm{mm}\cdot\mathrm{min}^{-1}$	50	0	0.15 ± 0.08
				0.19 ± 0.08
			5	0.55 ± 0.08
				0.51 ± 0.08
	3 h		5	0.50 ± 0.08
				0.28 ± 0.08
1300	$2.5~\mathrm{mm}\cdot\mathrm{min}^{-1}$	50	0	0.28 ± 0.09
				0.26 ± 0.10
			5	0.79 ± 0.08
				0.73 ± 0.08
	3 h		5	1.01 ± 0.09
				0.80 ± 0.09
1200	$2.5~\mathrm{mm}\cdot\mathrm{min}^{-1}$	50	0	0.16 ± 0.08
				0.14 ± 0.08
			5	0.61 ± 0.08
				0.49 ± 0.08
	3 h		5	1.24 ± 0.09
				1.60 ± 0.09

the highest porosity. However, this is not confirmed by visual inspection, which in turn explains a possible incorrect porosity measurement due to high open porosity. The higher density according to Archimedes also indicates bubble-free compaction of the green body during sintering and the associated transparency of the sample. In addition, the surface of the samples is not polished, which explains the partially poorer appearance of some areas of the samples.

3.2. Sintering results

Due to the influence of the sintering temperature, feed rate and holding time as well as the gas atmosphere in the furnace, different sintering results of the molded parts could be achieved, see Table 3.

The increasing sintering temperature and the associated higher energy input increase the diffusion processes and viscous flow, thereby accelerating the sintering process [12,13]. At 1200 °C, the samples are not yet vitrified; vitrification of the center of the sample was only achieved by holding it in the hot zone for 3 hours. With a holding time of 3 h at 1400 °C, the sample again shows more bubbles than at 1300 °C. This could be due to defluorination of the sample and the associated bubble formation. The samples with a feed rate of 2.5 mm·min⁻¹ exhibit different sintering behavior due to the gas atmosphere. Sintering was improved by the low fluorine-containing furnace atmosphere, resulting

L. Krämer and G. Falk Open Ceramics 23 (2025) 100834

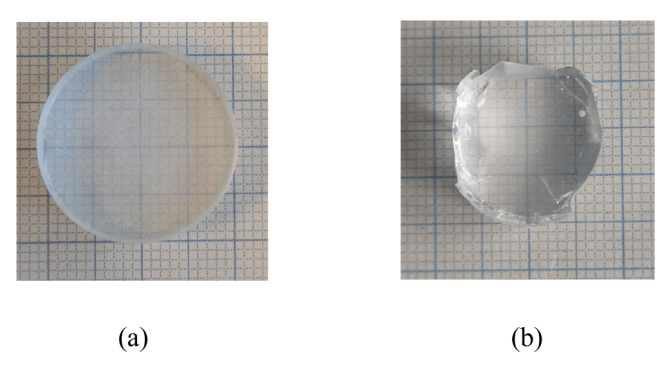


Fig. 4. The OX50-samples before (a) and after (b) the hot isostatic pressing.

in a bubble-free sintered body at 1400 °C. In a pure nitrogen atmosphere, however, there are still some bubbles in the sintered body. Fig. 3 shows the SEM images of the molded bodies sintered under a fluorine-containing atmosphere at 1400 °C. The bubbles of the samples held at 3 h are clearly visible, whereas the sample with a feed rate of 2.5 $\rm mm\cdot min^{-1}$ only shows very isolated bubbles.

In addition, EDX analyses of the sintered bodies were carried out to investigate the influence of gas-phase fluorination and the sintering conditions on the fluorine concentration. The fluorine concentration of the EDX analyses are listed in Table 4.

When holding the sample in the hot zone, the highest fluorine concentrations were reached at 1200 °C with approx. 1.60 ma.- %. As the temperature increases, the fluorine concentration decreases again and defluorination predominates. In the samples with a feed rate of 2.5 $\rm mm\cdot min^{-1}$, the samples at 1300 °C show the highest fluorine concentrations. This means that the stronger influence of defluorination can only be detected at 1400 °C when the sample is moved in the furnace. The fluorine-containing atmosphere in the furnace significantly increases the fluorine concentration in all samples. A high fluorine gas concentration is therefore important during the sintering of the samples, but fluorine corrosion and safety must be taken into account.

3.3. Hot isostatic pressing

Fig. 4 shows the OX50 sample before (a) and after (b) the hot isostatic pressing. The HIP process greatly reduced and eliminated the bubbles that were previously clearly visible. Only individual bubbles are still visible. This can also be seen in the light microscope images in Fig. 5. The bubble density has been greatly reduced. As not all bubbles have been completely removed, the process conditions for HIP must be adjusted.

To confirm the optical impression, transmission spectra in the range from 400 nm to 800 nm of the samples were recorded with the UV–VIS spectrometer, see Fig. 6.

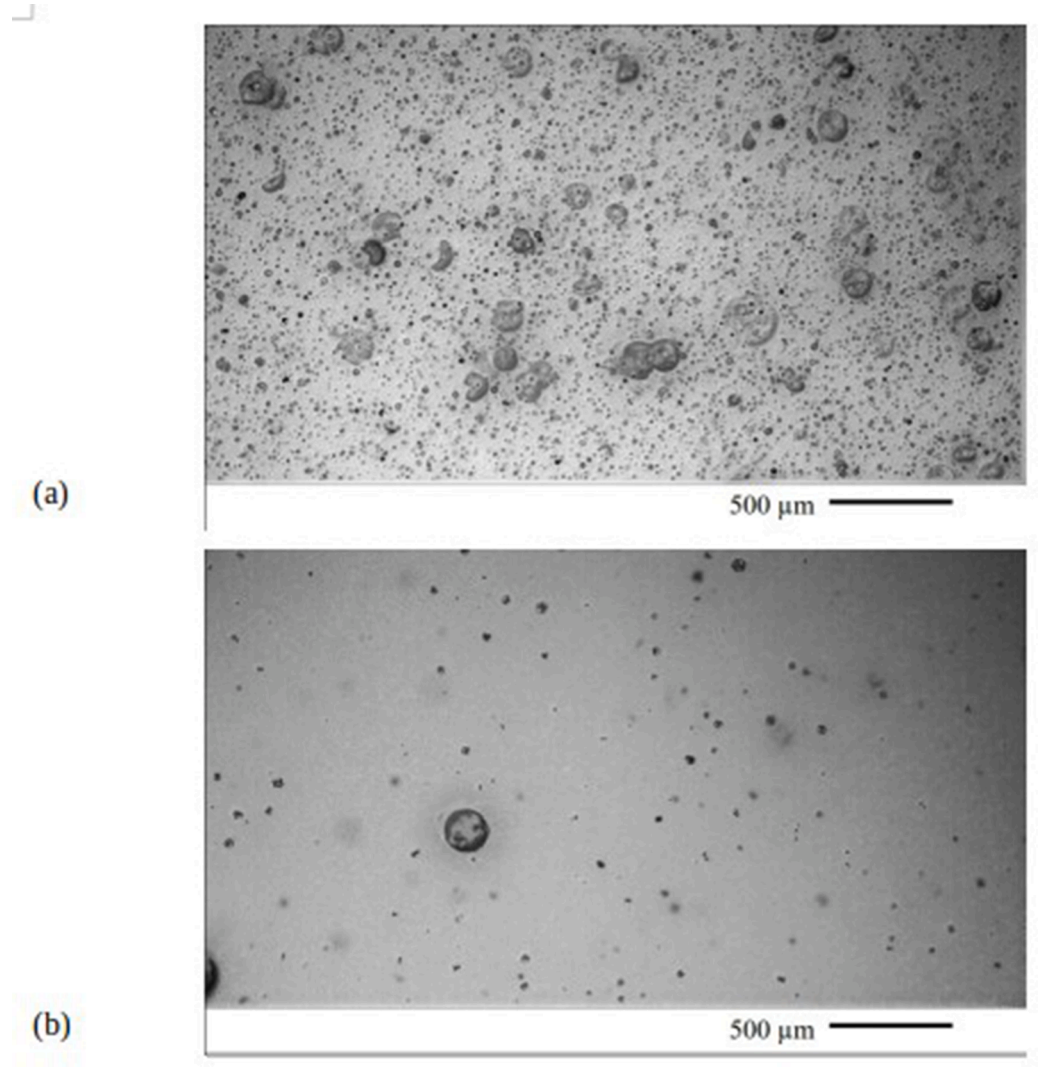


Fig. 5. Light microscopic images of the samples OX50-samples before (a) and after (b) the hot isostatic pressing with multifocus.

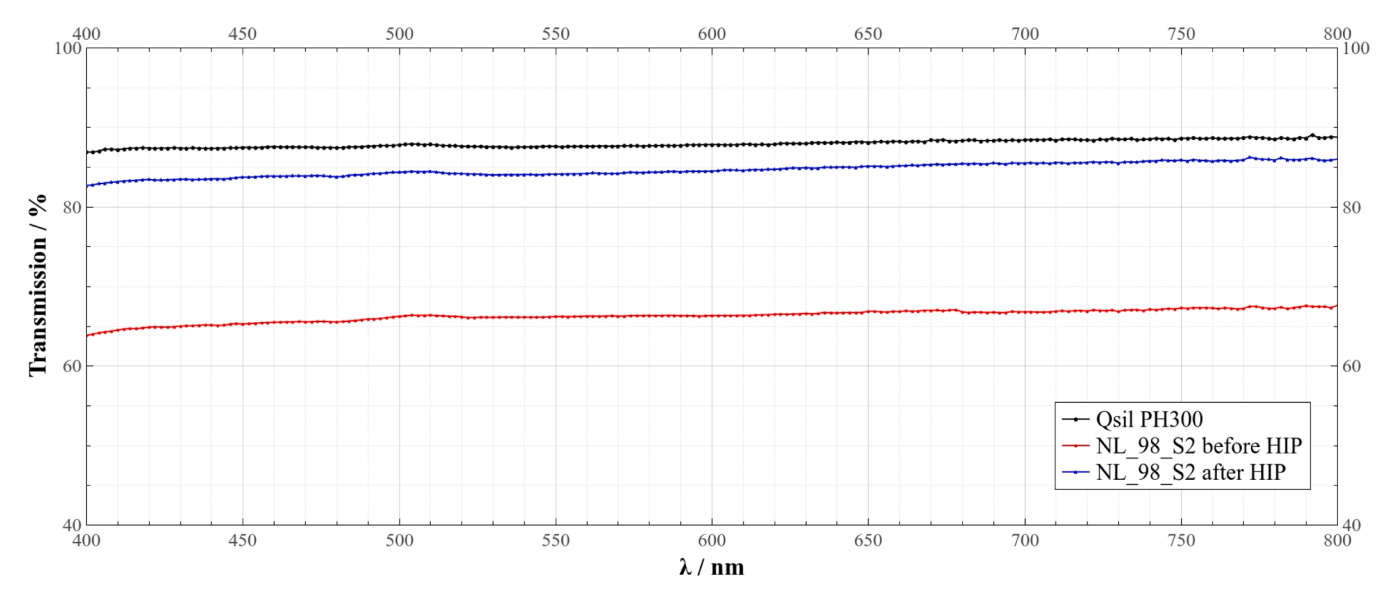


Fig. 6. UV-VIS-spectra of the OX50 samples before and after hot isostatic pressing and the silica glass Qsil PH300.

The significant increase in transmission from approx. 67% before the HIP process to approx. 86% after the HIP process at 800 nm can be seen. As a reference, a transmission spectrum of the silica glass PH300 (QSIL GmbH) was also recorded. The reference sample has a transmission of approx. 88%. Thus, the conditions of hot isostatic pressing are not yet optimal, but already lead to a strong bubble reduction and thus to a transmission increase of 19% and a transmission that is only 2% below the reference sample.

4. Conclusions

Optimized dispersion preparation with ultrasonic post-treatment and sieving of the dispersions enables green bodies with high densities and low porosities to be produced. This enables transparent sintering of the green bodies in the tubular flow reactor at temperatures as low as 1480 $^{\circ}\text{C}$. By combining this with gas phase fluorination with SF₆, additional fluorination of the sintered bodies can be achieved. The achievable fluorine concentration depends on the sintering temperature and the sintering conditions. The defluorination process increases with increasing sintering temperature and leads to a reduction in the fluorine concentration in the sample. Hot isostatic pressing enables complete compaction of the sintered bodies, which leads to an increase in the transmission of the samples. This makes it possible to carry out fluorination and sintering of the bodies at lower temperatures and then achieve complete compaction through the HIP process.

CRediT authorship contribution statement

L. Krämer: Writing – original draft, Visualization, Validation, Project administration, Methodology, Data curation, Conceptualization. **G. Falk:** Supervision, Conceptualization, Resources, Writing – review & editing.

Declaration of competing interest

The authors declare that they have no known competing financial

interests or personal relationships that could have appeared to influence the work reported in this paper.

References

- M. Saad, Fluoride glass fiber: state of the art, in: Proc. of SPIE 7316, Fiber Optic Sensors and Applications VI, 2009 73160N, https://doi.org/10.1117/12.824112.
- [2] K. Schuster, S. Grimm, A. Kalide, J. Dellith, M. Leich, A. Schwuchow, A. Langner, G. Schötz, H. Bartelt, Evolution of fluorine doping following the REPUSIL process for the adjustment of optical properties of silica materials, Opt. Mater. Express 5 (2015) 887, https://doi.org/10.1364/OME.5.000887.
- [3] T. Chartier, Optical fibers, in: J.D. Hrsg von Musgraves, J. Hu, L. Calvez (Eds.), Springer Handbook of Glass, Springer International Publishing, Cham, 2019, pp. 1405–1439, https://doi.org/10.1007/978-3-319-93728-1_41. Springer Handbooks.
- [4] J. Lucas, F. Smektala, J.L. Adam, Fluorine in optics, J. Fluorine Chem.. 13th Eur. Symposium Fluorine Chemistry (ESFC-13) 114 (2) (2002) 113–118, https://doi. org/10.1016/S0022-1139(02)00016-7.
- [5] B.J. Skutnik, B. Foley, K.B. Moran, High-numerical-aperture silica core fibers, in: Proc. SPIE 5317, Optical Fibers and Sensors for Medical Applications IV, 2004, https://doi.org/10.1117/12.529467
- [6] J. Ballato, H. Ebendorff-Heidepriem, J. Zhao, L. Petit, J. Troles, Glass and process development for the next generation of optical fibers: a review, Fibers 5 (2017) 11, https://doi.org/10.3390/fib5010011.
- [7] M. Kyoto, M. Ito, Y.u.a. Ishiguro, Study of fluorine doping during vapour phase axial deposition sintering process, J. Mater. Sci. 31 (9) (1996) 2481–2486, https://doi.org/10.1007/BF01152965.
- [8] E.M. Rabinovich, D.M. Krol, N.A.u.a. Kopylov, Retention of fluorine in Si- lica gels and glass*, J. Am. Ceramic Society 72 (7) (1989) 1229–1232, https://doi.org/10.1111/j.1151-2916.1989.tb09712.x.
- [9] E. Wiberg, N. Wiberg, A.F. Holleman, Anorganische Chemie. 103. Auf- lage, De Gruyter, Berlin; Boston, 2017.
- [10] B.B. Harbison, I.D. Aggarwal, Hot isostatic pressing of fluoride glasses, J. Non Cryst. Solids 161 (1993) 7–9, https://doi.org/10.1016/0022-3093(93)90658-K.
- [11] J. Bauch, R. Rosenkranz, Physikalische Werkstoffdiagnostik: Ein Kompendium, Springer, Berlin Heidelberg, 2017, https://doi.org/10.1007/978-3-662-53952-1.
- [12] Sintern, H. Salmang, H.K Scholze, 7. Auflage, Springer Verlag, 2007, pp. 313–380. ISBN: 978-3-540-63273-3.
- [13] D. Tramosljika, Sinterverhalten Einer Bei Niedrigen Temperaturen Sinternden Keramik und Der Einfluss von Silber auf Deren Sinterverhalten, Universität Stuttgart, 2010, https://doi.org/10.18419/opus-1284.